# Demonstration of spontaneous symmetry breaking in self-modulated ring resonators

Yoonhyuk Rah [*] and Kyoungsik Yu [†]

*School of Electrical Engineering, Korea Advanced Institute of Science and Technology, KAIST, Daejeon 34141, Republic of Korea*

(Received 2 September 2023; accepted 15 January 2024; published 4 March 2024)

The demonstration of spontaneous symmetry breaking in a system consisting of a pair of self-modulated ring resonators is performed. In addition, the critical effect of thermal heating induced by optical absorption is studied, where experimental results with numerical calculations reveal that optical absorption contributing as an optical nonlinearity is greatly dominant over the optical Kerr effect under certain operation speeds, depicting a significant impact on the system performance. Our analysis of the operation characteristics outlines important characteristics of self-modulated nonlinear resonators and their function as an optical binary state system.

DOI: 10.1103/PhysRevResearch.6.013234

## I. INTRODUCTION

Spontaneous symmetry breaking has long been an attractive study in optical systems [1–5], where various nonlinear effects have been exploited to generate binary state operations. Among a variety of systems, optical resonators [6–9] have been widely used, where the large power confinement enabled by high-quality factors along with the optical Kerr nonlinearity of commonly used dielectric materials, e.g., silicon and silicon nitride, yields spontaneous symmetry breaking above a certain pump power threshold depending on the system characteristics.

Theoretically proposed in a previous model [10], symmetry breaking can be induced in an integrated photonic system consisting of a pair of self-modulating optical resonators interacting with each other via a feedback loop, leading to a binary state operation to potentially represent an Ising model spin. Above a certain pump power threshold, the circulating intensities in the pair of resonators show symmetry breaking due to self-phase modulation and the optical Kerr effect. In this article, we report the experimental demonstration of symmetry breaking in a system consisting of self-modulated ring resonators. In addition, we discover the unaccounted critical role of thermal heating induced by optical absorption, and we analyze its critical impact on operation characteristics.

Device fabrication was performed with LIGENTEC's AN800 MPW run, where an 800-nm-thick stoichiometric silicon nitride ($Si_3N_4$) layer was utilized for sufficient mode confinement in the waveguides, leading to low propagation losses and high $Q$-factor resonators with optical Kerr nonlinearities. The schematic of the photonic circuit layout is similar to the previous work [10] and shown in Fig. 1(a), consisting of a pair of resonators and three directional couplers (DC1-3) connected by a feedback loop and a Mach-Zehnder interferometer (MZI) structure. Signal ports for the input, pump, and output power are indicated by black arrows. Ring resonator radii were set to 150 μm to obtain sufficient intrinsic $Q$-factors of over $2 \times 10^6$, leading to a free spectral range (FSR) of approximately 150 GHz. Metal heaters are located above each resonator for thermo-optic resonance frequency tuning. Additional heaters are used for inducing a $\pi$-phase shift in the upper bus waveguide and for phase control in the feedback loop between DC2 and DC3.

The pump signal is introduced into the feedback loop via DC3, which is then split equally by DC1 into both arms of the MZI structure. The scattering matrix of DC1 (S1) and DC2 (S2) must be set to meet the condition $S_1 \times S_2 = I$. This can be easily achieved by setting $S_1 = S_2$ and implementing a $\pi$ phase shift in the upper waveguide arm of the MZI structure. For DC1 and DC2 set to yield 50/50 cross/through coupling ratios along with identical ring resonator resonances, equal power will be introduced into both resonators. The equations based on coupled mode theory governing the resonator amplitudes $A_{i=1,2}$ are written as follows:

$$\frac{dA_{i=1,2}}{dt} = -\left[\kappa_e + \kappa_l + i\left(\Delta_{0i=1,2} + \chi\left|A^2_{i=1,2}\right|\right)\right] \times A_{i=1,2} - \sqrt{\kappa_e} u_{i=1,2} \quad (1)$$

with resonator external loss linewidth $\kappa_e$, internal loss linewidth $\kappa_l$, nonlinear coefficient $\chi$ [11], input bus waveguide signals $u_{i=1,2}$, and initial detuning $\Delta_{0i=1,2}$. Below the pump power threshold, the system lies in a stable symmetric status, where equal nonlinear effects occur in both resonators. In the total absence of noise along with ideal conditions, the system will enter an unstable symmetric state above the pump power threshold. With the introduction of a small input signal, the optical power in the arms of the MZI structure will show a slight imbalance depending on the input-pump phase relationship, further leading to slightly different amounts of nonlinear shifting in the resonator. Figure 2(a) shows the numerically

[*] yoonhyuk94@kaist.ac.kr
[†] ksyu@kaist.ac.kr

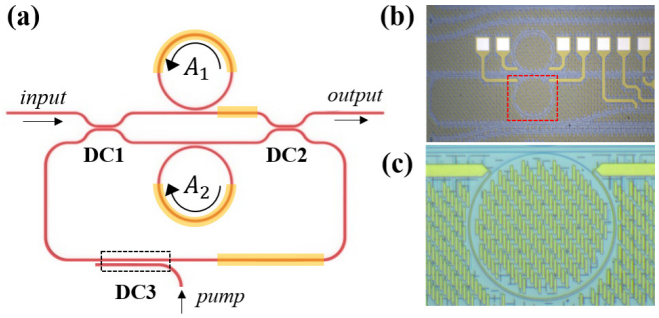


FIG. 1. (a) Schematic of the demonstrated model. Heater locations are displayed as yellow traces. (b) Optical microscope image of the fabricated chip. (c) Magnified optical image of region shown in red box in (b). Filling patterns can be seen.

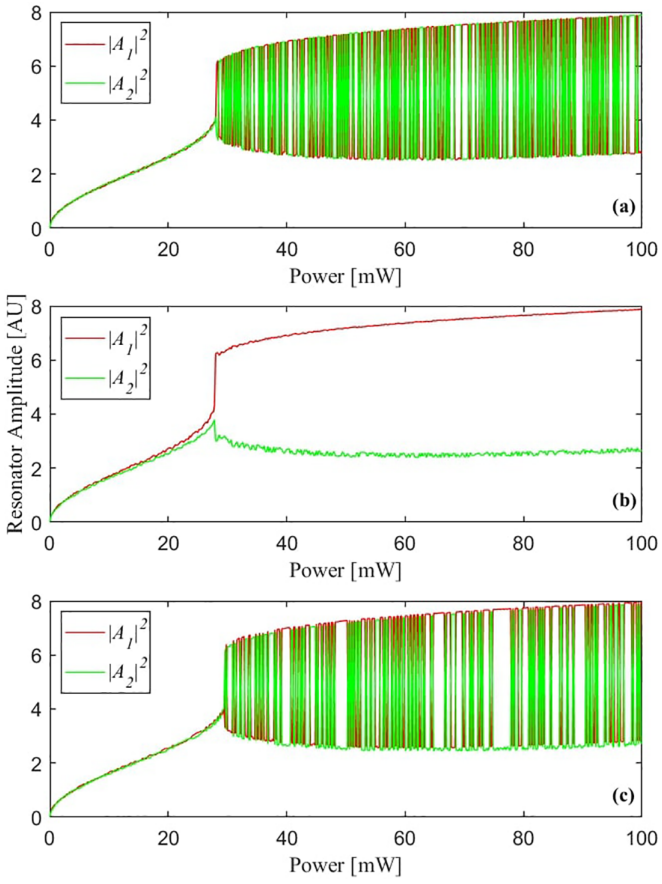


FIG. 2. (a) Steady-state amplitude of resonators for different pump powers in the ideal case. (b) Steady-state amplitude of resonators for different pump powers when cross/through power coupling ratios for DC1 and DC2 are set to 48/52. (c) Steady-state amplitude of resonators for different pump powers when cross/through power coupling ratios for DC1 and DC2 is set to 52/48. Initial resonance detunings are set to −1.37 and −1.33 GHz for resonators 1 and 2, respectively. For each case of different pump power, the relative phase between the input and pump signal was set to random values for verifying the accessibility of both bistable states. The cross/through power coupling ration of DC3 was set to 30/70.

TABLE I. Table of parameters used in our numerical calculations.

| Parameter | Value | Description |
|---|---|---|
| $\lambda$ | 1.55 (μm) | wavelength |
| $\kappa_e$ | $4.3432 \times 10^8$ (Hz) | external loss |
| $\kappa_l$ | $4.3432 \times 10^8$ (Hz) | internal loss |
| $n_2$ | $2.4 \times 10^{-19}$ | Kerr index |
| $n_0$ | 1.997 | effective index |
| $A_{\text{eff}}$ | $1.176 \times 10^{-12}$ | mode area |
| $r$ | 150 (μm) | ring radius |
| $\chi$ | 2.5403 | nonlinear coefficient |

calculated steady-state amplitudes of the resonator powers. Above the pump threshold, this self-phase modulation process will eventually induce symmetry breaking where one resonator gains a larger power than its counterpart. This mechanism will eventually alter the optical power leaving DC2 and reentering the feedback loop, thus leading to one of the bistable states determined by the pump-input signal phase relationship. For numerical calculations, the pump signal phase is set to 0, while the phase of the input signal is randomly changed for different pump powers to verify its accessibility for both bistable states.

However, in real-world fabrications, an ideal 50/50 splitting directional coupler can be challenging to fabricate. In addition, resonators will have slightly different resonance frequencies. Depending on the imbalance of these components, the system can reach only one of the bistable states regardless of the input-pump relationship. Figure 2(b) shows the numerically calculated steady-state amplitudes of the resonator powers where the cross/through coupling power ratio of DC1 and DC2 is set to 52/48. The upper waveguide in the MZI structure is consistently pumped with more power, consistently leading to the bistable state where the upper resonator amplitude ($A_1$) shows a larger value than the lower resonator ($A_2$) above the pump threshold. This bias can be compensated by implementing phase shifters in the ring resonators or tunable directional couplers where adjustments can be applied to make conditions similar to the ideal case. In our setup, metal thermal heaters were installed above the ring resonators for resonance tuning as shown in Fig. 1(a). Figure 2(c) shows the resonator steady-state amplitudes when the resonance detuning of the resonators 1 and 2 is set to −1.37 and −1.33 GHz to compensate the imbalanced cross/through coupling power ratio of 52/48 guiding more power into the waveguide coupled to resonator 1. Both bistable states are accessed for random input-pump phase relationships, restoring the balance in a matter similar to the situation in Fig. 2(a). Parameters used in our calculations are shown in Table I.

## II. EXPERIMENTAL ANALYSIS

To determine the operation status and functionality of the system, we analyzed the output power response as a function of pump power. The pump power was generated by a tunable laser (TOPTICA CTL1550) and boosted by an optical amplifier (Keopsys KPS-BT2-C-30-PF) to obtain sufficient optical powers above the threshold. Numerical calculations were performed by the Runge-Kutta fourth-order method to estimate

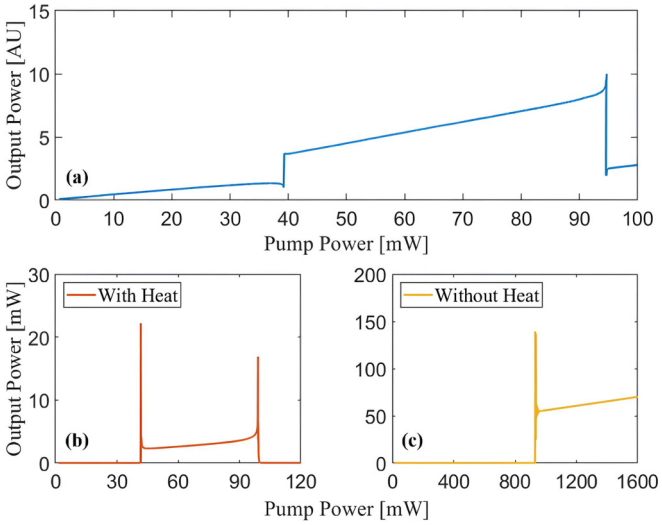


FIG. 3. (a) Output power as a function of pump power experimentally observed with the ramp-up method. (b) Numerical calculations of output power under the existence of thermal heat absorption. (c) Numerical calculations of output power under the absence of thermal heat absorption.

the pump power threshold and initial detuning. To control the pump power, a voltage signal from a function generator (Keysight 33120A) was applied to a variable optical attenuator (VOA, Thorlabs V1550A). Power coupling ratios of the directional couplers were measured in adjacent test structures, which were investigated to be 44/56 (cross/through) for DC1 and DC2. To compensate for this imbalance, the resonance of resonator 2 was additionally blueshift-detuned. For a fixed center laser wavelength, the initial resonance detunings of the resonators were measured by dithering the laser wavelength via the laser controller piezoscan. To eliminate the effect of any nonlinear resonance shifts, the pump power was set to sub-μW levels. In addition, the phase shift in the upper waveguide of the MZI-structure was set to 0 for easy observation of the resonance dips in the output port signal. After analysis of the resonators' resonance relative to the center laser wavelength, the initial resonance detuning was altered by changing the piezovoltage controlling the center wavelength. During our initial analysis, symmetry breaking of the system indicated by an abrupt increase of output power was never observed. The event of the system entering one of the possible bistable states was only observed when the resonance of the resonators was further blueshifted from the laser frequency, corresponding to a much larger resonator resonance-laser detuning than the value estimated through our numerical calculations. This was easily achieved by redshifting the laser frequency, rather than controlling the metal heaters on both resonators.

Figure 3(a) shows the measured output power as a function of the pump power when gradually increased from 0 to 100 mW in a time step of 20 ms. The initial frequency detuning of resonators 1 and 2 relative to the laser was −3.33 and −3.55 GHz, respectively. An abrupt increase in the output power is observed near $P_{\text{pump}} = 40$ mW, indicating a symmetry-broken status and successful operation of the system. Above the pump power threshold, the amplitude of the circulating modes in the pair of ring resonators generates a sufficient resonance redshift originating from the optical nonlinearities, where an imbalance between the mode intensities leads to a large detuning split. To verify the operation of the proposed system, we compared the experimental results with our numerical calculations where parameters were set to yield similar conditions to our fabricated device and operation wavelength. Based on setup parameters implemented in our numerical calculations, a significantly larger threshold value of over 900 mW was derived [Fig. 3(c)], depicting a remarkable difference from our experimental results. In addition, the second transition point indicated by an abrupt output intensity decrease was not observed up to calculations of pump power over 2000 mW. These results imply that either an unaccounted nonlinear effect is present or the foreknown optical Kerr effect shows a much stronger value. However, the possibility of a larger optical Kerr nonlinearity provides an unrealistic solution since it requires a strength nearly 23.5 times larger than its expected value of $2.4 \times 10^{-19}$ m$^2$/W, depicting a value even larger than crystalline silicon [12]. A highly probable and more convincing solution can be ascribed to the optical absorption in the resonator, where additional heat generation [13] can contribute to a refractive index increase and thus larger nonlinear redshifts. Absorption-induced temperature variation [14] is implemented into our calculations where the detuning term is modified as follows:

$$\Delta_{i=1,2} = \Delta_{0_i=1,2} + \chi |A_{i=1,2}|^2 + \omega_0 \frac{dn}{dT} \frac{(T_{i=1,2} - T_0)}{n_0} \quad (2)$$

with pump frequency $\omega_0$, initial detuning $\Delta_{0i=1,2}$, temperature $T$, initial temperature $T_0$, thermo-optic coefficient (TOC) $dn/dT$, and initial effective index $n_0$. Based on these modifications, we recalculated the output power response shown as the curve in Fig. 3(b). The output power response shows a greatly improved match portraying both the abrupt output power increase and decrease observed in our demonstrated analysis, proposing a reasonable solution to the untaken effect in the original model. The first transition point near $P_{\text{pump}} =$ 40 mW where the output power shows an abrupt increase indicates the system entering a symmetry-broken status, which is in good agreement with our experimental results. The small but observable output power prior to the threshold can be ascribed to nonideal phase settings in the waveguides and imperfections in the directional couplers. The fast fluctuating ringing phenomenon near the transition points has been observed in other high-$Q$ resonators [15] which appear as large spikes near the transition points but are not experimentally detected due to the limited speed of the photodiodes. Thermal heating due to material absorption is governed by the optical absorption coefficient $\alpha$, the thermo-optic coefficient $dn/dT$, and the thermal time constant $\tau$ [14]. A value of $2.45 \times 10^{-5}$/K was used for the thermo-optic coefficient.

Unlike the instantaneous optical Kerr effect [16], temperature-dependent index variation is a relatively slower process where its characteristic timescales are typically longer than several microseconds [13]. This implies that under operation time cycles of several milliseconds, the optical absorption thermal effect may overwhelm the optical Kerr effect and act as the main nonlinearity in the symmetry-breaking

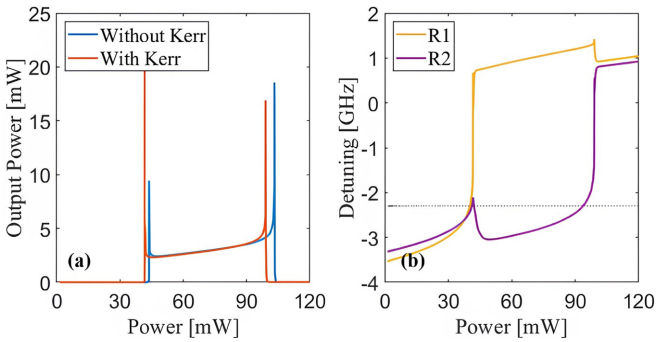


FIG. 4. (a) Output power response with (orange) and without (blue) the optical Kerr effect when the pump power is increased. Both cases show similar patterns where the presence of the optical Kerr effect slightly lowers the transition point values. (b) Resonator detuning response when the pump power is increased.

process. Figure 4(a) shows numerical calculations of the output power response with parameters set to yield a similar condition as in our experimental demonstrations. To speed up the calculations, we applied an appropriate multiplier factor to the thermal time constant $\tau$ and the run time. The curves indicate the response in the presence (orange) and absence (blue) of the optical Kerr effect. Both situations show similar pump power transition points and trajectories, implying that the temperature-dependent index change due to the optical absorption is dominant over the optical Kerr effect, and is the main issue driving the symmetry-breaking procedure. The presence of the optical Kerr effect slightly lowers both transition point pump levels since it also is a nonlinearity but only shows relatively smaller effects. Figure 4(b) shows the numerically calculated resonators' detuning response with the optical Kerr effect taken into, showing a strong bifurcation at the first transition point. Both values converge to a similar value at the second transition point where the system fails to maintain a symmetry-broken status. A noteworthy point is that both state transitions occur at the instance where either one of the resonator detunings reaches a value of approximately $-2.3$ GHz, indicated by the black dashed line. We believe this value is related to the resonators' $Q$-factors and Lorentzian-shaped transmission spectrum [17], where systems with different nonlinear dimensions will lead to different detuning transition points.

The steady-state output response was evaluated by introducing a constant pump power at $t = 0$ s and measuring the output power after $t = 1$ s. Figure 5(a) shows the steady-state response, where the functional operation regime is observed at pump powers ranging from 48 to 53 mW. The nonzero output power prior to the transition point at 48 mW can be ascribed to nonideal phase shifts and component variations. The operational regime from 48 to 53 mW shows a much smaller range relative to the ramp-up method along with a much smaller pump value corresponding to the second transition point. This can be straightforwardly ascribed to increased amounts of optical absorption heat generation in the steady-state measurement method. The increased redshift due to thermal absorption pulls the collapsing point of the symmetry breaking status to lower pump power levels. On the contrary, even in the presence of excess thermal redshifts,

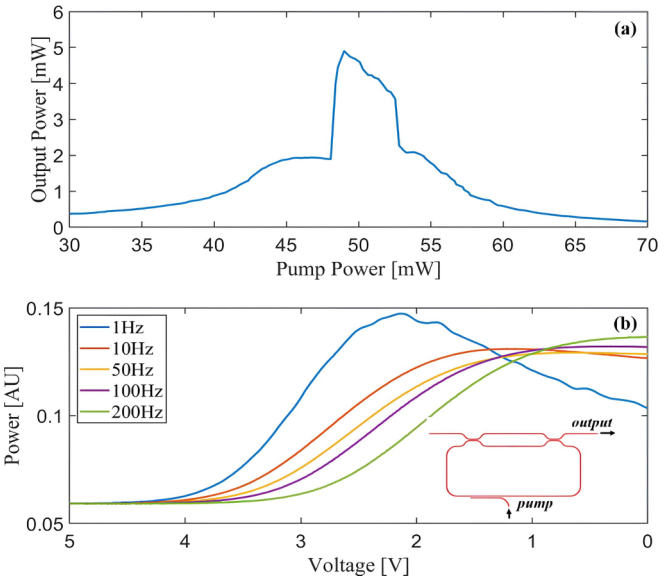


FIG. 5. (a) Experimentally observed steady-state output power as a function of pump power. (b) Output port signal response as a function of the voltage applied to the VOA for different frequencies. The inset shows the setup and how the measurements were performed where interaction from the ring resonators is omitted.

the first transition point pump power shows a slightly larger value relative to the transition point observed in the ramp-up method, portraying a contradicting matter since additional nonlinear shiftings will induce symmetry breaking at a lower pump level. We believe this discordance can be attributed to the excess nonlinear shifts induced by thermal absorption in the feedback loop at longer duration times. The structure of the feedback loop resembles a large ring resonator which will also show thermal absorption at high powers. We test this matter by analyzing the output signal when modulating the pump signal at different frequencies. If the feedback loop is not affected by the slow thermal absorption process, its response to a pump signal with amplitude modulation will not vary for different modulation frequencies. To test this matter, a triangle pulse wave ranging from 0 to 5 V was applied to the VOA (Thorlabs V1550A) to control the pump power at different modulation speeds from 1 to 200 Hz. The laser frequency was detuned far away from the resonators' resonances to prevent nonlinear interaction from the pair of resonators. Figure 5(b) shows the output power response of the feedback loop when the pump power is modulated at different frequencies. In a single cycle where the voltage is decreased from 5 to 0 V, the pump power coupled into the feedback loop increases from 0 mW to approximately 100 mW. The curve corresponds to the trajectory of the output power depending on the pump power controlled by the voltage applied on the VOA. The differing amount of thermal absorption in a single cycle at slow speeds (blue curve) and relatively faster speeds (green curve) generates different amounts of nonlinear shifts leading to nonidentical phase shifts and thus varying transmission properties. Since the feedback loop phase shift applied in the method applied to obtain data shown in Fig. 3 was set to meet conditions where smaller amounts of thermal absorption take

place, additional adjustments are required to generate equal phase settings in the steady-state configuration.

## III. CONCLUSION

In conclusion, we have experimentally demonstrated the spontaneous symmetry breaking of a pair of self-modulated ring resonators in a photonic integrated circuit platform. We reveal the unaccounted effect of thermal absorption and analyze its critical influence on the system operation. The large redshifting property of the thermal heat generation greatly reduces the pump power threshold but also limits the upper operational pump power regime where large powers generate a significant amount of heat overwhelming the optical Kerr effect and degrade stable operation. In timescales of milliseconds, the thermal absorption effect is largely responsible over the optical Kerr effect for driving the bifurcation procedure. Faster operation speeds in the nano-microsecond regime can reduce optical absorption and enhance the influence of the optical Kerr effect but will require adjusted resonator detuning ranges and improved $Q$-factor resonators to incorporate quicker responses. Nevertheless, the system itself proposes a functional binary-state system where the optical absorption effect can be employed to lower the operation threshold. Furthermore, we believe the steplike output power response can be exploited for other applications such as all-optical regeneration [18,19] and spiking neuromorphic processing [20,21] where a small change in pump power can lead to a relatively larger increase in output power. With enhanced $Q$-factor resonators, we believe the operation performance can be improved to yield faster response times for high-speed applications.

## ACKNOWLEDGMENTS

This work was supported by Samsung Research Funding and Incubation Center of Samsung Electronics under Project No. SRFC-IT2002-04.

## APPENDIX: THERMAL HEATING RESPONSE OF FEEDBACK LOOP

To test the thermal heating response of the feedback loop, we measured the output power while modulating the pump power at different frequencies. To eliminate the effect of the resonators, the laser frequency was adjusted far away from the resonance wavelengths. To assure the response does not originate from the VOA itself, we tested the frequency response of the VOA. Figure 6(a) shows the output power response as a function of applied voltage when swept from 0 to 5 V and decreased back to 0 V. Despite slight shifts in terms of applied voltage, the response shows a consistent pattern along with equal maximum and minimum signal power. The voltage signal was set to generate a triangular pulse wave ranging from 0 to 5 V. Due to the frequency bandwidth, tests were conducted up to 200 Hz. Figure 6(b) shows the output signal response, showing different patterns for varying modulation frequencies. In addition, the maximum signal powers differ depending on the modulation frequency, implying that different amounts of thermal heating lead to altering amplitudes and phase responses.

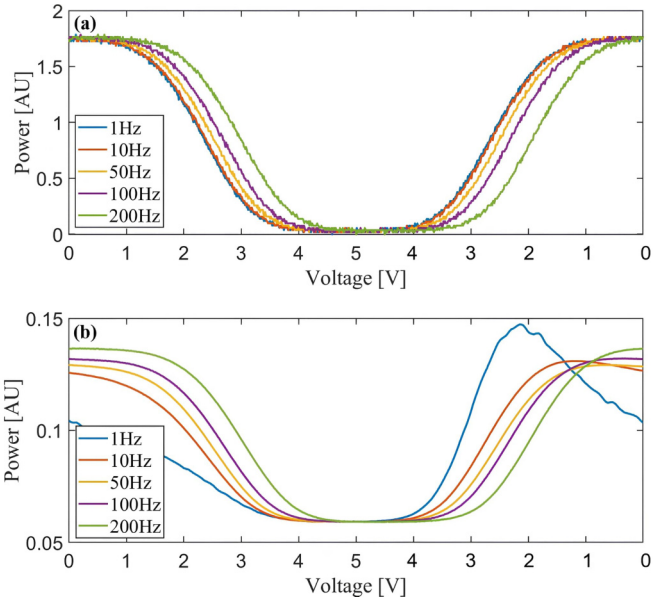


FIG. 6. (a) VOA output power response at different modulation frequencies. (b) Output signal power response of the feedback loop for different modulation frequencies. Different switching times yield different amounts of thermal heating, consequently leading to different phase responses.

[1] P. Hamel, S. Haddadi, F. Raineri, P. Monnier, G. Beaudoin, I. Sagnes, A. Levenson, and A. M. Yacomotti, Spontaneous mirror-symmetry breaking in coupled photonic-crystal nanolasers, Nat. Photon. **9**, 311 (2015).

[2] B. Maes, P. Bienstman, and R. Baets, Symmetry breaking with coupled Fano resonances, Opt. Express **16**, 3069 (2008).

[3] F. Copie, M. T. M. Woodley, L. Del Bino, J. M. Silver, S. Zhang, and P. Del'Haye, Interplay of polarization and time-reversal symmetry breaking in synchronously pumped ring resonators, Phys. Rev. Lett. **122**, 013905 (2019).

[4] M. Kang, F. Liu, and J. Li, Effective spontaneous $PT$-symmetry breaking in hybridized metamaterials, Phys. Rev. A **87**, 053824 (2013).

[5] B. Maes, M. Soljačić, J. D. Joannopoulos, P. Bienstman, R. Baets, S.-P. Gorza, and M. Haelterman, Switching through symmetry breaking in coupled nonlinear micro-cavities, Opt. Express **14**, 10678 (2006).

[6] L. Del Bino, J. M. Silver, S. L. Stebbings, and P. Del'Haye, Symmetry breaking of counter-propagating light in a nonlinear resonator, Sci. Rep. **7**, 43142 (2017).

[7] L. Hill, G.-L. Oppo, M. T. M. Woodley, and P. Del'Haye, Effects of self-and cross-phase modulation on the spontaneous symmetry breaking of light in ring resonators, Phys. Rev. A **101**, 013823 (2020).

[8] M.-A. Miri, E. Verhagen, and A. Alù, Optomechanically induced spontaneous symmetry breaking, Phys. Rev. A **95**, 053822 (2017).

[9] M. T. M. Woodley, J. M. Silver, L. Hill, F. Copie, L. Del Bino, S. Zhang, G.-L. Oppo, and P. Del'Haye, Universal symmetry-breaking dynamics for the Kerr interaction of counterpropagating light in dielectric ring resonators, Phys. Rev. A **98**, 053863 (2018).

[10] N. Tezak, T. Van Vaerenbergh, J. S. Pelc, G. J. Mendoza, D. Kielpinski, H. Mabuchi, and R. G. Beausoleil, Integrated coherent Ising machines based on self-phase modulation in microring resonators, IEEE J. Sel. Top. Quantum Electron. **26**, 1 (2019).

[11] T. J. Kippenberg, A. L. Gaeta, M. Lipson, and M. L. Gorodetsky, Dissipative Kerr solitons in optical microresonators, Science **361**, eaan8083 (2018).

[12] N. K. Hon, R. Soref, and B. Jalali, The third-order nonlinear optical coefficients of Si, Ge, and $Si_{1-x}Ge_x$ in the midwave and longwave infrared, J. Appl. Phys. **110**, 011301 (2011).

[13] T. Carmon, L. Yang, and K. J. Vahala, Dynamical thermal behavior and thermal self-stability of microcavities, Opt. Express **12**, 4742 (2004).

[14] J. Zhu, M. Zohrabi, K. Bae, T. M. Horning, M. B. Grayson, W. Park, and J. T. Gopinath, Nonlinear characterization of silica and chalcogenide microresonators, Optica **6**, 716 (2019).

[15] S. Trebaol, Y. Dumeige, and P. Féron, Ringing phenomenon in coupled cavities: Application to modal coupling in whispering-gallery-mode resonators, Phys. Rev. A **81**, 043828 (2010).

[16] H. Rokhsari and K. J. Vahala, Observation of Kerr nonlinearity in microcavities at room temperature, Opt. Lett. **30**, 427 (2005).

[17] K. J. Vahala, Optical microcavities, Nature (London) **424**, 839 (2003).

[18] R. Salem, M. A. Foster, A. C. Turner, D. F. Geraghty, M. Lipson, and A. L. Gaeta, All-optical regeneration on a silicon chip, Opt. Express **15**, 7802 (2007).

[19] S. J. Madden, D.-Y. Choi, D. A. Bulla, A. V. Rode, B. Luther-Davies, V. G. Ta'eed, M. D. Pelusi, and B. J. Eggleton, Long, low loss etched $As_2S_3$ chalcogenide waveguides for all-optical signal regeneration, Opt. Express **15**, 14414 (2007).

[20] T. S. Rasmussen, Y. Yu, and J. Mork, All-optical non-linear activation function for neuromorphic photonic computing using semiconductor Fano lasers, Opt. Lett. **45**, 3844 (2020).

[21] A. Jha, C. Huang, and P. R. Prucnal, Reconfigurable all-optical nonlinear activation functions for neuromorphic photonics, Opt. Lett. **45**, 4819 (2020).